

Structure, Scaling, and Performance of Natural Micro- and Nanocomposites

Sacheen Bekah · Reza Rabiei · Francois Barthelat

© Springer Science+Business Media, LLC 2011

Abstract Natural materials boast remarkable mechanical performances in some cases unmatched by their synthetic counterparts, and for this reason, they have become an inspiration for the development of new materials. In high-performance natural materials such as nacre, bone, or teeth, stiffness and toughness are achieved with the staggered microstructure, where stiff inclusions of high aspect ratio are embedded in a softer matrix. While the modulus and strength of the staggered structure is well understood, fracture toughness and scaling remains unclear. In this work, a fracture model based on the fundamental micromechanics of the staggered structure is presented. The model captures crack bridging and process zone toughening, and explicitly shows how these toughening processes are the most efficient with high concentrations of small tablets of high aspect ratio. In particular, a desirable non-steady cracking regime can be achieved with specific requirements for structure and interface properties, which are presented in detail. These attractive toughening mechanisms are only possible if the tablets themselves do not fracture. The benefits of small size have been explored in the past, but here, we show for the first time how the effects of a stress singularity generated by the junctions between the tablets can be alleviated by the softer interfaces, provided that a “soft wrap” condition is met. The models provide new insights into the optimization and scaling of natural and biomimetic composites.

Keywords Nacre · Bone · Biological composites · Fracture toughness · Micromechanics · Biomimetics

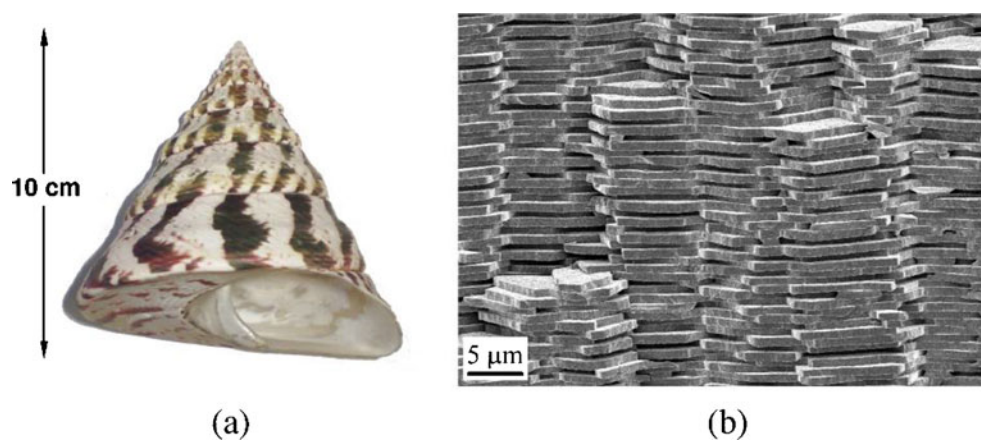
S. Bekah · R. Rabiei · F. Barthelat (✉)
Department of Mechanical Engineering, McGill University,
817 Sherbrooke Street West,
Montreal, Quebec, Canada H3A 2K6
e-mail: francois.barthelat@mcgill.ca

1 Introduction

Natural materials exhibit remarkable combinations of strength, modulus, and toughness [1], and for this reason, they are now serving as models for the design of biomimetic materials [2–5]. Among hard biological materials, nacre boasts remarkable structural performances and has become the archetype of biomimetic models. Nacre is part of a two-layer armor system that forms the shell of mollusks such as top shell (Fig. 1a). Nacre is hard and stiff, but it is its toughness which is the most impressive: nacre is three orders of magnitude tougher than the mineral it is made of (in energy terms) [1], a level of “toughness amplification” which is currently not matched by any synthetic composite [6]. The remarkable performance of nacre is the result of a sophisticated microstructure, where microscopic mineral tablets are arranged in a three-dimensional brick wall and bonded by softer but tougher organic layers (Fig. 1b). This “staggered structure” of stiff inclusions of high aspect ratio is also found in teeth, spider silk, and cellulose fibers, so that it has been identified as one of the “universal” patterns found in natural materials [7].

The primary mode of deformation of the shell when subjected to an external aggression is bending. As a result, the function of the nacreous layer is to resist tensile loading along the tablets, which are roughly parallel with the surface of the shell. The resulting micromechanics in tension can be described as a “tension–shear” chain, where tablets are under tensile stress and the interface undergoes shear [8–10]. If the interfaces are allowed to yield before the tablets break, then the tablets will “slide” on one another, generating large deformations (Fig. 2a). This mechanism has been the basis of predictive models for the strength, modulus, and toughness of staggered composites [9, 11, 13–15]. The representative volume element shown

Fig. 1 Top shell (*Trochus niloticus*) (a) and its nacreous structure (b)



in Fig. 2b is often used to capture these micromechanisms [9, 13]. Under tension, the tablets mainly carry tensile stresses while the interfaces are loaded in shear. Some proteins at the interface can undergo significant viscoplastic deformation with energy dissipation because of the sacrificial bonds they contain [16]. In addition to the effect of the organic phase, nanometer-sized asperities existing on the surface of the aragonite tablets have been shown to enhance the overall mechanical properties by strengthening the organic/mineral interface [17, 18]. The mineral bridges connecting the neighboring tablets also contribute to the strength of the interface through inducing crack deflection and crack arresting [19].

Interestingly, the “tension–shear” and sliding mechanisms were also identified in the bone at the microscale [20]. Under tension, mineralized collagen fibrils glide on one another, the sliding being also mediated by protein molecules. These molecules present sacrificial bonds as an extra source of energy dissipation, comparable to those observed at the interface of nacre interface [16, 21].

The size and scaling of the structure of natural composites is an important question in the context of biomimetics. The staggered inclusions in bone, nacre, or

teeth are micron or submicron in size, and according to the Griffith criterion of fracture mechanics, decreasing the size of flaws results in high tensile strength. Since a given component can only contain flaws that are smaller than its dimensions, smaller objects are stronger. Following these principles, Currey [22] used the toughness of calcite (computed from its surface energy) to estimate the crack length that would fracture the tablets under a tensile stress corresponding to the strength of nacre (100 MPa). By comparing the result (2 μm) with the thickness of the tablets (0.5 μm), Currey concluded that the tablets cannot contain a crack long enough to propagate from the stresses experienced in nacre. More recently, this idea was further developed by Gao et al. [11] who proposed that nanoscale inclusions cannot contain flaws large enough to propagate following Griffith principles of fracture mechanics. For minerals used in natural materials, they determined that inclusions smaller than 30 nm become insensitive to the presence of flaws and that their strength approaches the theoretical strength of a perfect crystal. While this estimate is close to the length scale of hydroxyapatite inclusions in bone, it is one order of magnitude smaller than the size of the tablets in nacre. Other researchers have argued that small inclusions remain fragile and that it is the hierarchical construction of natural materials which provides them with their remarkable macroscopic properties [23]. A comprehensive understanding of the fracture of natural composites is still missing.

The goal of this article was to examine structure–toughness relationships in staggered composites and to provide unified guidelines for the design of biomimetic composites based on the staggered structure. In particular, the effect of mineral concentration, aspect ratio, and size on stiffness, strength, and toughness are explored. Existing micromechanics-based models for stiffness and strength are discussed, and a new model for fracture is presented. The non-steady regime of cracking is found to be highly desirable for these structures, and the conditions for this regime are for the first time stated as a function of the

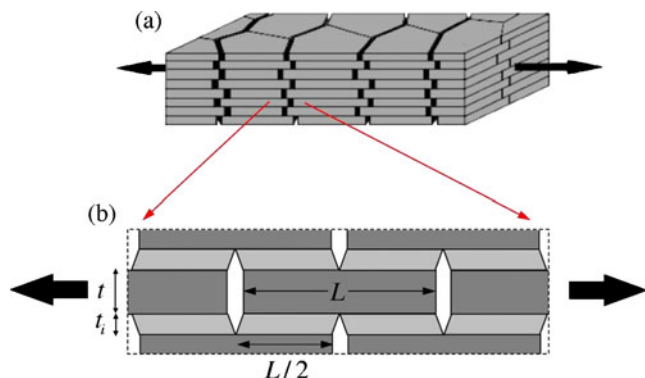


Fig. 2 a The “tablet sliding” mechanism in nacre generates large deformation. b Its micromechanics often captured using a small two-dimensional RVE [8, 11, 12]

microstructure and properties of the interfaces. In the last section of the article, the fracture of the tablet is predicted, which leads to the concept of the organic interfaces acting as “soft wraps” around the tablets, protecting them from external stresses. The outcome of this analysis is a set of scaling laws for biological and bio-inspired composites, which can be used to duplicate deformation and fracture mechanisms at larger scales.

2 Modulus and Strength

Much work was devoted to the elasticity and strength of the staggered structure along the direction of the tablets [8, 9]. The starting point for these models is the representative volume element shown in Fig. 2b. For soft and thin interfaces compared to the tablets, a good approximation of the modulus of the composite is given by [8, 24]:

$$\frac{1}{E} \approx \frac{1}{\phi E_m} + 4 \frac{1}{\rho^2} \frac{1-\phi}{\phi^2} \frac{1}{G_i} \quad (1)$$

where E_m is the Young's modulus of the mineral, G_i is the shear modulus of the interface, ϕ is the volume concentration of the mineral tablets, and $\rho = L/t$ is their aspect ratio. Equation 1 properly predicts that stiffer interfaces and/or stiffer tablets lead to higher overall stiffness. In terms of structure, stiffer composites can be achieved by increasing the mineral concentration or by increasing the aspect ratio of the tablets. For large tablet aspect ratios, the model converges toward the Voigt composite model (rule of mixture):

$$\lim_{\rho \rightarrow \infty} (E) = E_{\text{voigt}} = \phi E_m \quad (2)$$

Interestingly, the modulus E converges rapidly towards E_{voigt} as the aspect ratio of the tablets is increased. For nacre with $E_m \approx 100$ GPa, $G_i \approx 1$ GPa, and $\phi \approx 0.95$, the modulus reaches a value of $0.9 E_{\text{voigt}}$ for a tablet aspect ratio of $\rho = 14$, which is close to the actual aspect ratio of nacre ($\rho \approx 10$). For $\rho \approx 10$, Eq. 1 predicts $E_m \approx 60$ GPa, which is consistent with tensile experiments [14]. For nacre, the shear deformation of the interface and the tensile deformation of the tablets contribute to the overall stiffness by the same amount (the two terms in the right-hand side of Eq. 1 have similar values).

The strength of the composite is controlled by the shear strength of the interfaces. Assuming a perfectly plastic interface (no hardening), when the structure yields, the shear stress transferred across the interfaces is uniform and equal to τ_s . The tensile strength of the composite is then simply given by:

$$\sigma_s = \frac{1}{2} \rho \tau_s \quad (3)$$

For nacre, $\rho \approx 10$ and $\tau_s \approx 25$ MPa lead to $\sigma_s \approx 125$ MPa, which is in the range of strengths measured experimentally [10, 13, 17, 22]. The variations of stiffness and strength as a function of microstructure can be conveniently visualized on a material property chart [12]. Equation 3 demonstrates that greater strength can be achieved by increasing τ_s or ρ [10, 11]. The aspect ratio of the tablets cannot, however, be increased indefinitely because the shear force transmitted through the interface is converted to tension in the tablets, which may lead to tablet fracture. This important limitation is addressed at the end of the article.

3 Toughness

The toughness of the staggered composite is more difficult to predict because there are several mechanisms that operate concurrently to impede crack advance. It is evident from the examination of a fracture surface (Fig. 1b) that the crack circumvents the tablets following the interfaces. This requires soft interfaces and strong tablets, as described at the end of this article. As the crack progresses, the tablets are pulled out, which generates closure tractions on the crack faces, similar to crack bridging by fibers (Fig. 3b). The analysis of this mechanism leads to a simple expression for the toughness J_0 generated by bridging only [12]:

$$J_0 = \frac{1}{2} \rho J_i \quad (4)$$

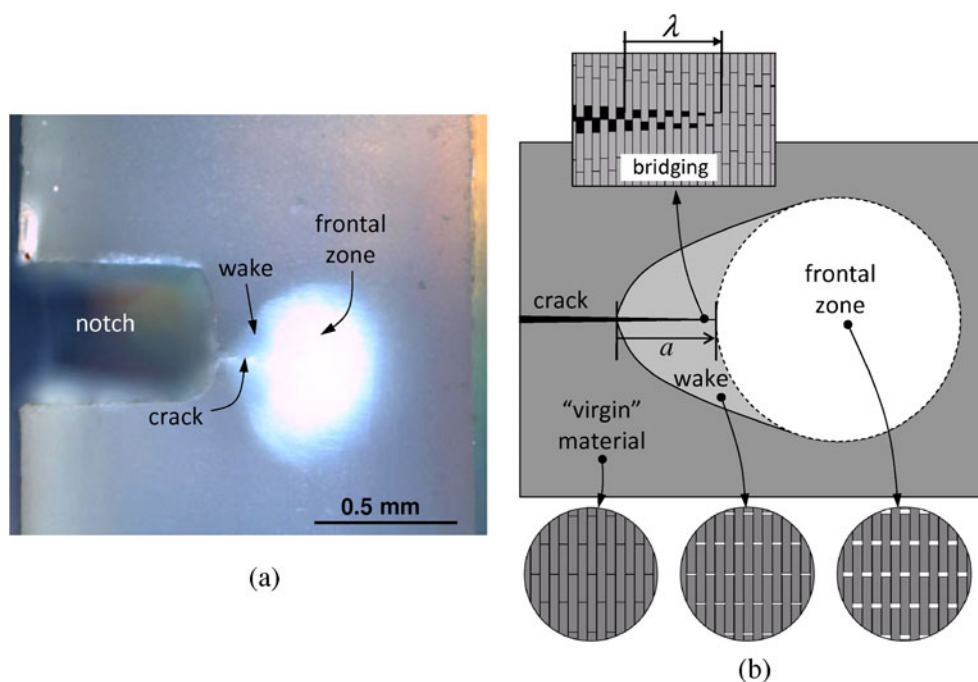
where J_i is the interface toughness and ρ is the aspect ratio of the tablets. The toughness of the interfaces is therefore “amplified” by ρ . The length of the cohesive zone associated to bridging can be written (Fig. 3) [12]:

$$\lambda = \frac{\pi}{8} \frac{J_0 E}{\sigma_s^2} \quad (5)$$

In addition to bridging, high stresses near the crack generate a process zone which consists of a frontal zone and a wake. In the frontal zone ahead of the crack, massive tablet sliding occurs, which can be readily observed in an experiment because the material whitens (Fig. 3a), an optical effect similar to stress whitening in polymers. Once the crack runs through the initial frontal zone, the material unloads and some of the deformation is recovered, leaving a wake behind the crack tip (Fig. 3a).

The amount of energy dissipated in the process of loading/unloading the material as the crack advances by a small increment can be relatively easily calculated with the assumption that the crack has propagated over a distance sufficient to generate a wake of uniform width (steady-state

Fig. 3 **a** Optical micrograph of a crack propagating in top shell nacre. The whitening in the frontal zone is an indication of tablet sliding. **b** Schematic of the various deformation regions developing around the advancing crack



regime). In this case, the result does not depend on the shape of the frontal zone, and the overall toughness is given by [12]:

$$J = \frac{J_0}{1 - \alpha} \tag{6}$$

where α is a “process zone parameter” [12]. Assuming rigid tablets and a Dugdale cohesive law at the interfaces, α can be written:

$$\alpha = \frac{1}{4} \left(\frac{1}{t} \frac{\phi^2}{1 - \phi} \frac{G_i J_i}{\tau_S^2} - 1 \right) \tag{7}$$

While the length of the bridging region can be written:

$$\lambda = \frac{\pi}{16} \rho \frac{\phi^2}{1 - \phi} \frac{G_i J_i}{\tau_S^2} \tag{8}$$

where (ϕ, t) are the tablet concentration and tablet thickness (microstructural parameters) and (G_i, J_i, τ_S) the shear modulus, toughness, and shear strength of the interfaces (materials parameters), respectively. Process zone toughening therefore further amplifies toughness, as established previously for polymers toughening with rubber particles [25]. For the staggered composite, the amount of amplification is clearly controlled by the process zone parameter α , with greater values for α leading to higher overall toughness. Equation 6, however, also shows that if $\alpha \geq 1$, the assumption of steady-state cracking breaks down and the predicted toughness has no physical value (the amplification becomes negative). For $\alpha \geq 1$, transient crack-

ing, where the width of the wake changes with crack advance, must therefore be considered. Using Eq. 7, the condition for non-steady cracking is:

$$5t \frac{1 - \phi}{\phi^2} \leq \frac{G_i J_i}{\tau_S^2} \tag{9}$$

This regime is relevant for nacre, where the size of the frontal zone/wake system observed in fracture experiments clearly increases as the crack advance (Fig. 3a). In this non-steady-state regime, the contribution of the process zone to toughening is more challenging to obtain than for the steady case because the result depends on the shape of the frontal zone [26]. It is possible, however, to obtain a simple solution by assuming that the frontal zone is circular (Fig. 3b). Using this approximation, the amount of energy dissipated over a small crack increment can be evaluated, which leads to a differential equation that can be solved numerically [12]. The results from solving this equation properly predict that the fracture toughness reaches a steady-state value for cases where $\alpha < 1$. In contrast, for cases where $\alpha > 1$, the model predicts that fracture toughness increases indefinitely with crack advance and never reaches a steady value.

Figures 4, 5, and 6 show the results from the model in the form of crack resistance curves where the overall toughness (J) and the crack extension (a , Fig. 3) are non-dimensionalized with respect to the interface properties. From these figures, the effect of each microstructural parameter (ϕ, t , and ρ) on the overall toughness can be systematically explored. In Fig. 4, increasing ρ while maintaining t and ϕ constant results in a longer cohesive

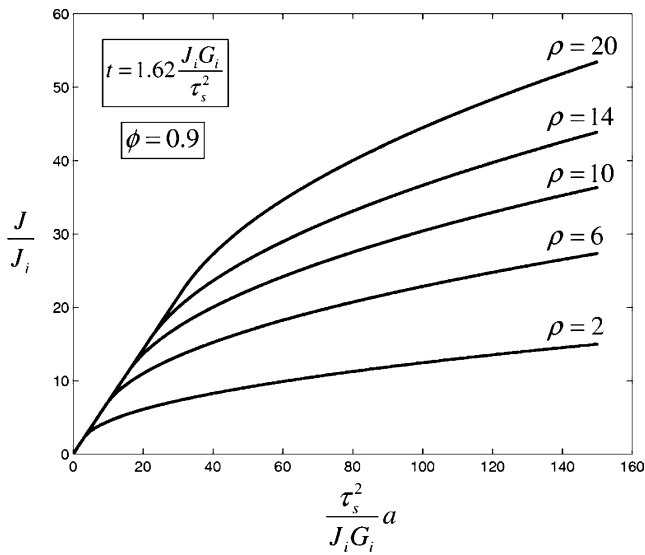


Fig. 4 Effect of tablet aspect ratio on the toughness, for a fixed tablet size and concentration. The values of toughness and crack extension are normalized with respect to the properties of the organic interface

zone λ , in a larger bridging toughness J_0 , in larger process zone toughening, and in higher toughness amplification overall. Decreasing the microstructure size t while maintaining ρ and ϕ constant has no effect on the cohesive zone λ and on the bridging toughness J_0 ; however, it leads to significant increases in process zone toughening and to higher overall toughness amplification (Fig. 5). Finally, increasing the concentration of the mineral phase ϕ while maintaining ρ and t constant increases the length of the cohesive zone λ significantly, but has no effect on bridging toughness J_0 . Increasing ϕ leads to increased process zone toughening and to significantly higher overall toughness amplification (Fig. 6). All the plots display fracture

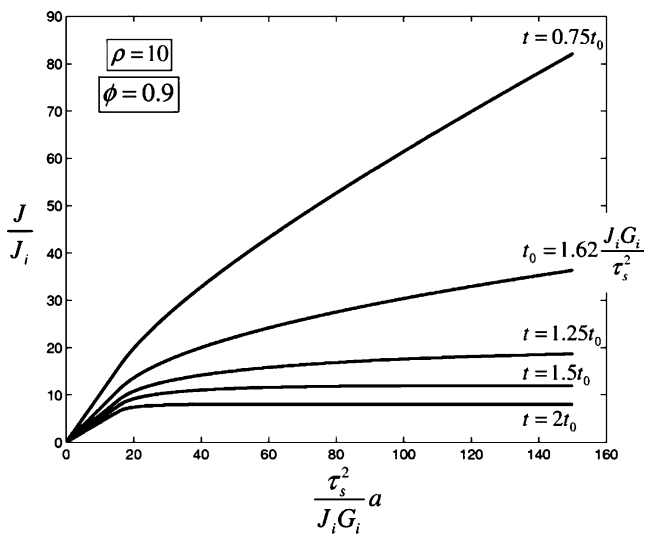


Fig. 5 Effect of tablet size on the toughness, for a fixed tablet aspect ratio and concentration

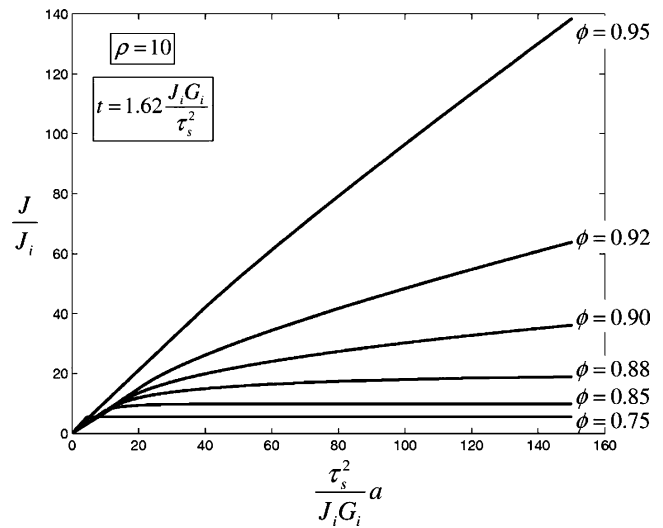


Fig. 6 Effect of mineral concentration on the toughness, for a fixed tablet aspect ratio and size

toughness which increases with crack advance. In general, a rising crack resistance is critical to crack stability and is highly beneficial to damage tolerance and to the mechanical reliability of the material [27]. This behavior is consistent with fracture experiments on nacre [28] and bone [29], which revealed rising crack resistance curves for those materials.

Typical structural and material properties of nacre lead to α values which are >1 ($1.15 < \alpha < 4$) [12]. Using the toughness model for the non-steady-state condition, the contribution of each toughening mechanism to the overall toughness of nacre can be evaluated. As a general trend, the bridging effect has its largest contribution to toughness for crack advances smaller than the steady-state cohesive length (Eq. 8). For longer cracks, bridging toughness remains constant while process zone toughening keeps growing continuously. The detailed contribution of each mechanism depends on the value of α . For example, for $\alpha = 1.15$, bridging contributes 40% of the overall toughness in non-steady bridging regime, whereas for $\alpha = 4$, this value drops to almost 5%. The predictions of the toughness model agree well with fracture experiments on nacre [12]. Figure 7 shows crack resistance curves obtained from fracture experiments on four different types of nacre. While nacre from top shell significantly toughens with crack advance, pen shell displays the least amount of toughening. Interestingly, the process zone in pen shell is much smaller in width compared with top shell [30], which highlights the important contribution of process zone toughening in nacre.

Closer examination of the microstructure of pen shell (Fig. 8a) reveals that it is composed of tablets which are thinner and longer (Fig. 8b) than those found in top shell (Fig. 1b), which in theory should lead to higher toughness.

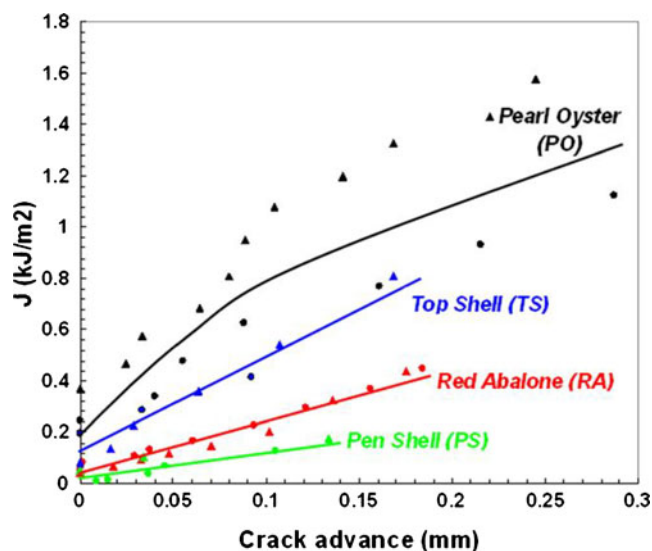


Fig. 7 Experimental crack resistance curves for four types of naces, including top shell *Trochus niloticus* and pen shell *Pinna nobilis* [30]

However, the fracture surface of pen shell (Fig. 8b) shows extensive tablet damage. The fracture of the tablets themselves inhibits the benefits of tablet sliding, which explains why pen shell is more brittle than top shell. The excessively high tablet aspect ratio in pen shell could stem from different evolutionary pressures exerted on the animal by its different ambient conditions compared with other shells, possibly resulting in a lessened demand for high fracture toughness. Nevertheless, pen shell provides an example where excessive aspect ratio results in tablets which cannot sustain the force transferred by shear stress at the interfaces.

4 Fracture of Individual Tablets

The case of pen shell illustrates an important condition for toughness: for the bridging and process zone toughening to operate, the tablets themselves must not break [2, 11, 13, 22]. Following the approach of Currey [22] and Gao et al. [11], we considered an edge crack

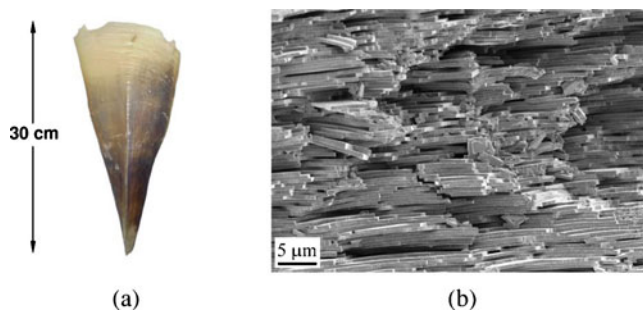


Fig. 8 Pen shell (*Pinna nobilis*) (a) and its nacreous structure (b) as exposed during a fracture test

extending halfway through the thickness, giving rise to the stress intensity factor:

$$K_I = 2.83\sigma_S\sqrt{\pi t/2} \quad (10)$$

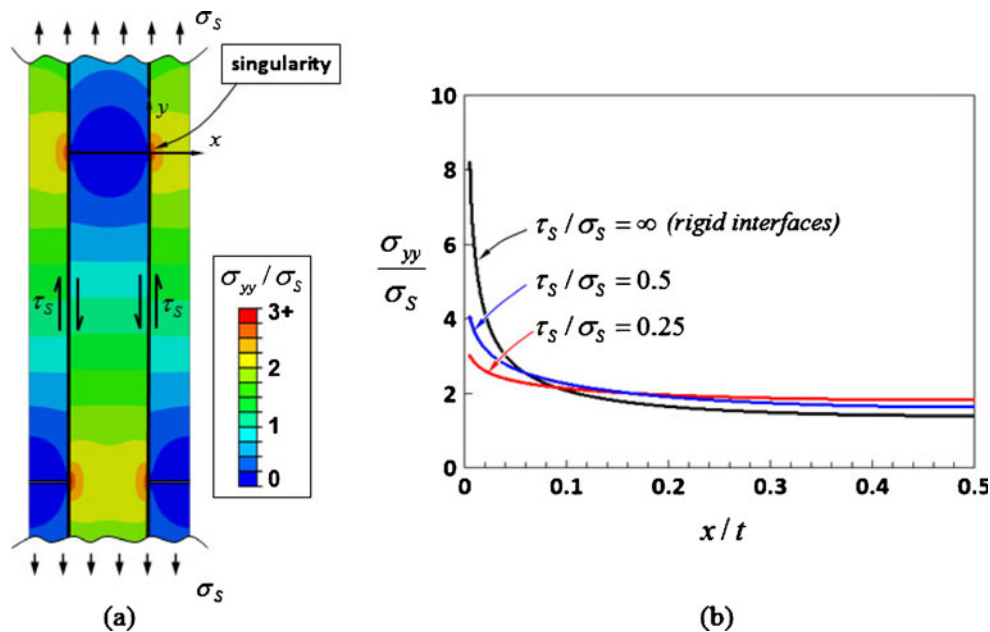
Using Eqs. 3 and 10 and writing the condition $K_I < K_{IC}$ in order to prevent tablet fracture:

$$\rho < 0.56 \frac{K_{IC}}{\tau_S\sqrt{t}} \quad (11)$$

Equation 11 therefore provides an upper bound for the aspect ratio of the tablets. In terms of design, larger aspect ratios can be achieved with tougher tablets (higher K_{IC}), softer interfaces (lower τ_S), and with smaller microstructures (smaller t). This prediction was also compared with actual observations for nacre. Using $K_{IC}=0.39$ MPa m^{1/2} for calcite [31], $\tau_S \approx 25$ MPa [14], and $t \approx 0.5$ µm [30], Eq. 11 predicts a maximum allowable aspect ratio of 12. This prediction is remarkably close to the actual aspect ratio of the tablets of red abalone or top shell (about 10). In contrast, the average aspect ratio of the tablets in pen shell is about 14, which may explain the massive tablet damage observed in that species.

While these models provide useful insight into the scaling of natural staggered structure, they assume that the stresses are uniform within the tablets. In reality, this is not the case, and in particular high tensile stresses exist near the ends of the junctions (region separating the ends of the tablets). This effect was investigated with finite element models of the small representative volume element (RVE) of Fig. 2b (version 6.8-3, ABAQUS, Inc., Providence RI). The tablets were modeled as linear elastic and cohesive elements were inserted at the interface between the tablets. The cohesive elements reached a constant stress τ_S after a short elastic region, following [14]. Plane strain condition was used, and periodic conditions were imposed on all sides of the model. The RVE was then stretched along the direction of the tablets to simulate tension. Figure 9a shows the stress distribution in the tablets. The highest stresses were found near the ends of the horizontal junctions. Further inspection revealed that these points are actually stress singularity, generated by shear tractions from the interface exerted in opposed direction near the tip of the junction. Figure 9b shows the normalized axial stress along the x -axis ahead of the junction using different shear strengths for the interface. For all cases, the stress is infinite at the junction tip, but the softer interfaces, by yielding, effectively reduce the severity of the singularity near the junction and redistribute stresses across the thickness of the tablets. Interestingly, the same effect can be achieved by keeping τ_S constant while increasing the aspect ratio ρ (recalling Eq. 3). For all cases, however, the singularity at the tip of the junctions between the tablets remains, and the

Fig. 9 **a** Axial stress contour in the RVE showing stress singularities near the ends of the junctions. **b** Axial stress distribution ahead of the junction



junctions therefore act as crack-like features. Interestingly, this system is similar to multilayered materials made of brittle layers bonded by ductile interfaces studied by Chan et al. [32].

A fracture mechanics criterion was used to predict the possible propagation of the crack-like junction into the adjacent tablet. For the case where the tip of a crack meets a softer interface, the energy release rate is not clearly defined and the J-integral cannot be used. Instead, approximate values for the stress intensity factors were obtained here by fitting the asymptotic stress solution to the stress profiles of Fig. 9b. The stress intensity was found to reach its highest value when the interfaces are only partially yielded, but it remains the same until the entire interface has yielded. The effect of microstructure on the maximum stress intensity factor in the tablets was then captured by generating a large number of RVEs with various parameters. Figure 10 shows the geometrical factor β (obtained by normalizing the measured stress intensity factor with the tensile strength of the RVE) as function of aspect ratio, for both rigid interfaces and perfectly plastic interfaces. The plot clearly shows that the yielding of the interfaces significantly decreases the stress intensity factor when compared with cases where the interface is rigid. For a small aspect ratio, β is high because the junctions form a dense two-dimensional array of staggered cracks that strongly interact. At $\rho = 4$, the rigid interface models reach the converged value 1.13, corresponding to an array of cracks equally spaced and lying along a line perpendicular to the direction of loading. For the case of perfectly plastic interfaces, β keeps decreasing when ρ is increased because the interfaces effectively redistribute stresses.

Further analysis revealed that the stress intensity factor in the tablets is proportional to τ_s . This can be expected since when the interfaces are fully yielded the tablets are only subjected to surface tractions of uniform magnitude τ_s . The results reduce then to:

$$K_I = 0.58\tau_s\sqrt{t} \tag{12}$$

It then becomes evident that the interfaces behave as “soft wraps” around the fragile tablets and that by yielding they reduce the stress intensity factor. Small tablet size (i.e., thickness) will also reduce K_I . Using Eq. 12 and setting $K_I < K_{IC}$ gives the “soft wrap” condition:

$$\frac{K_{IC}}{\tau_s\sqrt{t}} > 0.58 \tag{13}$$

This behavior is beneficial to prevent the crack-like junction from crossing the interface and fracturing the

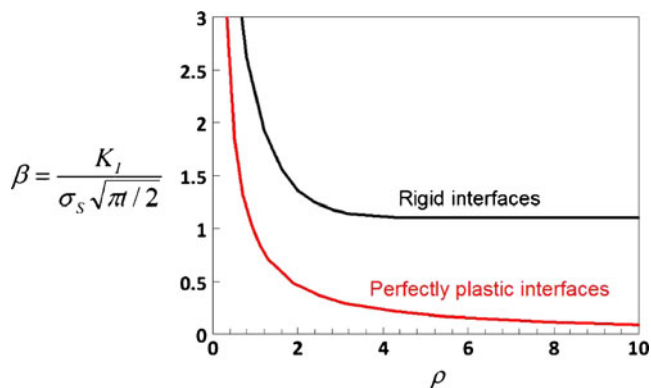


Fig. 10 Non-dimensional stress intensity factor in the tablets as function of tablet aspect ratio, shown for rigid interfaces and for perfectly plastic interfaces

tablets. In addition, in the event of an occasional individual tablet fracture, the soft wrap effect protects the adjacent intact tablets. Finally, the soft wrap effect protects the tablets from high stresses near defect, or at the tip of long cracks. In this context, the soft wrap effect becomes the condition for tablet pullout to dominate over tablet fracture at the tip of a long crack (Fig. 3a). For the case of nacre, taking $K_{IC}=0.39 \text{ MPa m}^{1/2}$ for calcite [31], $\tau_S \approx 25 \text{ MPa}$ [14], and $t=0.5 \text{ }\mu\text{m}$ for top shell [30], one finds $\frac{K_{IC}}{\tau_S \sqrt{t}} = 27.6$, which largely meets the “soft wrap” condition.

5 Conclusions

Biological materials demonstrate how useful combinations of stiffness, strength, and toughness can be achieved with the staggered microstructure. In particular, the models presented here demonstrate the importance of process zone toughening in this class of materials and discuss the conditions for optimum toughening in terms of microstructural parameters and interface properties. The model is also in good agreement with observations and measurements on nacre, the “archetype” of natural staggered composites. High stiffness, strength, and toughness can be achieved with high concentrations of small tablets with a high aspect ratio. These structural parameters seem to be optimum in nature possibly up to physical or biological limits: the tough structure of nacre inherits mineral tablets with high concentration (95 vol.%), small thickness (0.5 μm), and high aspect ratio. The latter parameter is, however, bounded by the strength of the tablets themselves to avoid the detrimental scenario of brittle tablet fracture. High aspect ratios also mean more overlap between tablets and higher tensile stresses transferred from the interface to the tablets. Here, we have shown for the first time the presence of stress singularity in the tablets, generated by the crack-like junctions. The severity of the singularity is, however, reduced by yielding of the soft interface, which leads to a new “soft wrap” condition. Soft interfaces therefore protect the brittle tablets from external stresses. While this phenomenon was hinted by previous work on natural nacre [33] and nacre-like synthetic material [3], it is formalized in this paper for the first time.

Overall, higher toughness, strength, and modulus can be achieved with smaller tablets. This result is consistent with previous findings, but in addition, this work proposes new relations between microstructure and interface properties that can be used to design and fabricate high-performance composites which combine the benefit of hardness and stiffness from hard inclusions with toughness, damage tolerance, and reliability. The ingredients of these composites do not need to be the same as in nacre; in fact,

aragonite is very brittle and should be avoided. The comprehensive guidelines presented here can then be used to determine optimum microstructures given a set of materials for the interfaces and tablets. Examples of material combinations used recently include alumina/chitosan [2] or HAP/epoxy [34]. Tight control on the microstructure (tablet arrangement, aspect ratio) remains a challenge at the micro- and nanoscale. In order to circumvent this difficulty, larger scale models of nacre have recently been proposed. For example, Espinosa et al. [5, 35] have recently developed a millimeter-scale “artificial nacre” fabricated using rapid prototyping techniques. Other types of large-scale “artificial nacre” based on friction have also recently been successfully developed [36, 37], where there is no material at the interface and the interaction of tablets is controlled by dry friction. Interestingly, debonding and friction also provide a powerful approach to redistribute stresses and protect the brittle tablets [32].

The models discussed in this article predict the overall deformation and fracture properties of biological or biomimetic composites based on simple, elementary mechanisms (tablet sliding, tablet fracture). This approach is similar to and complement ab initio molecular models used to predict material response at larger scales [38]. This “bottom-up” approach leads to materiomics [39], where the behavior of materials can be predicted at each relevant length scale and from first principles. The vision that drives these approaches is the design and optimization of materials at all length scales in order to duplicate the performance of natural materials and to achieve new combinations of properties useful for actual engineering applications.

Acknowledgments This work was supported by the Faculty of Engineering of McGill University, by the Natural Science and Engineering Council of Canada (Discovery Grant Program) and the Fonds Québécois de la Recherche sur la Nature et les Technologies (Programme Nouveaux Chercheurs).

References

1. Wegst, U. G. K., & Ashby, M. F. (2004). The mechanical efficiency of natural materials. *Philosophical Magazine*, 84, 2167.
2. Bonderer, L. J., Studart, A. R., Gauckler, L. J. (2008). Bioinspired design and assembly of platelet reinforced polymer films. *Science*, 319, 1069.
3. Munch, E., Launey, M. E., Alsem, D. H., Saiz, E., Tomsia, A. P., Ritchie, R. O. (2008). Tough, bio-inspired hybrid materials. *Science*, 322, 1516.
4. Barthelat, F. (2007). Biomimetics for next generation materials. *Philosophical Transactions of the Royal Society*, 365, 2907.
5. Espinosa, H. D., Rim, J. E., Barthelat, F., Buehler, M. J. (2009). Merger of structure and material in nacre and bone—Perspectives on de novo biomimetic materials. *Progress in Materials Science*, 54, 1059.

6. Ortiz, C., & Boyce, M. C. (2008). Materials science—Bioinspired structural materials. *Science*, *319*, 1053.
7. Buehler, M. J., Ketten, S., Ackbarow, T. (2008). Theoretical and computational hierarchical nanomechanics of protein materials: Deformation and fracture. *Progress in Materials Science*, *53*, 1101.
8. Jager, I., & Fratzl, P. (2000). Mineralized collagen fibrils: A mechanical model with a staggered arrangement of mineral particles. *Biophysical Journal*, *79*, 1737.
9. Kotha, S. P., Li, Y., Guzelsu, N. (2001). Micromechanical model of nacre tested in tension. *Journal of Materials Science*, *36*, 2001.
10. Ji, B. H., & Gao, H. J. (2004). Mechanical properties of nanostructure of biological materials. *Journal of the Mechanics and Physics of Solids*, *52*, 1963.
11. Gao, H. J., Ji, B. H., Jager, I. L., Arzt, E., Fratzl, P. (2003). Materials become insensitive to flaws at nanoscale: Lessons from nature. *Proceedings of the National Academy of Sciences of the United States of America*, *100*, 5597.
12. Barthelat, F., & Rabiei, R. (2011). Toughness amplification in natural composites. *Journal of the Mechanics and Physics of Solids*, *59*, 829.
13. Jackson, A. P., Vincent, J. F. V., Turner, R. M. (1988). The mechanical design of nacre. *Proceedings. Royal Society of London*, *234*, 415.
14. Barthelat, F., Tang, H., Zavattieri, P. D., Li, C. M., Espinosa, H. D. (2007). On the mechanics of mother-of-pearl: A key feature in the material hierarchical structure. *Journal of the Mechanics and Physics of Solids*, *55*, 225.
15. Gao, H. J. (2006). Application of fracture mechanics concepts to hierarchical biomechanics of bone and bone-like materials. *International Journal of Fracture*, *138*, 101.
16. Smith, B. L., Schaeffer, T. E., Viani, M., Thompson, J. B., Frederick, N. A., Kindt, J., et al. (1999). Molecular mechanistic origin of the toughness of natural adhesives, fibres and composites. *Nature (London)*, *399*, 761.
17. Evans, A. G., Suo, Z., Wang, R. Z., Aksay, I. A., He, M. Y., Hutchinson, J. W. (2001). Model for the robust mechanical behavior of nacre. *Journal of Materials Research*, *16*, 2475.
18. Katti, D. R., Pradhan, S. M., Katti, K. S. (2004). Modeling the organic–inorganic interfacial nanoasperities in a model bio-nanocomposite, nacre. *Reviews on Advanced Materials Science*, *6*, 162.
19. Song, F., & Bai, Y. L. (2003). Effects of nanostructures on the fracture strength of the interfaces in nacre. *Journal of Materials Research*, *18*, 1741.
20. Gupta, H. S., Seto, J., Wagermaier, W., Zaslansky, P., Boesecke, P., Fratzl, P. (2006). Cooperative deformation of mineral and collagen in bone at the nanoscale. *Proceedings of the National Academy of Sciences of the United States of America*, *103*, 17741.
21. Fantner, G. E., Hassenkam, T., Kindt, J. H., Weaver, J. C., Birkedal, H., Pechenik, L., et al. (2005). Sacrificial bonds and hidden length dissipate energy as mineralized fibrils separate during bone fracture. *Nature Materials*, *4*, 612.
22. Currey, J. D. (1977). Mechanical properties of mother of pearl in tension. *Proceedings. Royal Society of London*, *196*, 443.
23. Ballarini, R., Kayacan, R., Ulm, F. J., Belytschko, T., Heuer, A. H. (2005). Biological structures mitigate catastrophic fracture through various strategies. *International Journal of Fracture*, *135*, 187.
24. Liu G, Ji B, Hwang KC, Khoo BC. (2011). Analytical solutions of the displacement and stress fields of the nanocomposite structure of biological materials. *Composites Science and Technology*. doi:10.1016/j.compscitech.2011.03.011.
25. Evans, A. G., Ahmad, Z. B., Gilbert, D. G., Beaumont, P. W. R. (1986). Mechanisms of toughening in rubber toughened polymers. *Acta Metallurgica*, *34*, 79.
26. McMeeking, R. M., & Evans, A. G. (1982). Mechanics of transformation-toughening in brittle materials. *Journal of the American Ceramic Society*, *65*, 242.
27. Lawn, B. R. (1993). *Fracture of brittle solids*. New York: Cambridge University Press.
28. Barthelat, F., & Espinosa, H. D. (2007). An experimental investigation of deformation and fracture of nacre-mother of pearl. *Experimental Mechanics*, *47*, 311.
29. Ager, J. W., Balooch, G., Ritchie, R. O. (2006). Fracture, aging, and disease in bone. *Journal of Materials Research*, *21*, 1878.
30. Rabiei, R., Bekah, S., Barthelat, F. (2010). Failure mode transition in nacre and bone-like materials. *Acta Biomaterialia*, *6*, 4081.
31. Broz, M. E., Cook, R. F., Whitney, D. L. (2006). Microhardness, toughness, and modulus of Mohs scale minerals. *Am. Mineral.*, *91*, 135.
32. Chan, K. S., He, M. Y., Hutchinson, J. W. (1993). Cracking and stress redistribution in ceramic layered composites. *Mater. Sci. Eng., A*, *167*, 57.
33. Meyers, M. A., Lin, A. Y. M., Seki, Y., Chen, P. Y., Kad, B. K., Bodde, S. (2006). Structural biological composites: An overview. *JOM Journal of the Minerals Metals and Materials Society*, *58*, 35.
34. Deville, S., Saiz, E., Nalla, R. K., Tomsia, A. P. (2006). Freezing as a path to build complex composites. *Science*, *311*, 515.
35. Espinosa, H. D., Juster, A. L., Latourte, F. J., Loh, O. Y., Gregoire, D., & Zavattieri, P. D. (2011). Tablet-level origin of toughening in abalone shells and translation to synthetic composite materials. *Nature Communications*, *2*, 173.
36. Barthelat, F. (2010). Nacre from mollusk shells: A model for high-performance structural materials. *Bioinspiration & Biomimetics*, *5*, 8.
37. Barthelat, F., & Zhu, D. (2011). *Journal of Materials Research*, *26*(10).
38. Buehler, M. J., & Ackbarow, T. (2007). Fracture mechanics of protein materials. *Materials Today*, *10*, 46.
39. Buehler, M. J. (2010). Computational and theoretical materiomics: Properties of biological and de novo bioinspired materials. *Journal of Computational and Theoretical Nanoscience*, *7*, 1203.